

Cite this: *Chem. Sci.*, 2019, 10, 385

All publication charges for this article have been paid for by the Royal Society of Chemistry

# Structural control of polyelectrolyte/microemulsion droplet complexes (PEMECs) with different polyacrylates†

Miriam Simon, \*<sup>a</sup> Patrick Krause,<sup>a</sup> Leonardo Chiappisi, <sup>ab</sup> Laurence Noirez <sup>c</sup> and Michael Gradzielski \*<sup>a</sup>

The ionic assembly of oppositely charged polyelectrolyte–surfactant complexes (PESCs) is often done with the aim of constructing more functional colloids, for instance as advanced delivery systems. However, PESCs are often not easily loaded with a solubilisable due to intrinsic restrictions of such complexes. This question was addressed from a different starting point: by employing microemulsion droplets as heavily loaded surfactant systems and thereby avoiding potential solubilisation limitations from the beginning. We investigated mixtures of cationic oil-in-water (O/W) microemulsion droplets and oppositely charged sodium polyacrylate (NaPA) and determined structure and phase behaviour as a function of the mixing ratio for different droplet sizes and different  $M_w$  (NaPA). Around an equimolar charge ratio an extended precipitate region is present, which becomes wider for larger droplets and with increasing  $M_w$  of the NaPA. Static and dynamic light scattering (SLS and DLS) and small-angle neutron scattering (SANS) show the formation of one-dimensional arrangements of microemulsion droplets for polyelectrolyte excess, which become more elongated with increasing  $M_w$  (NaPA) and less so with increasing NaPA excess. What is interesting is a marked sensitivity to ionic strength, where already a modest increase to  $\sim 20$  mM leads to a dissolution of the complexes. This work shows that polyelectrolyte/microemulsion complexes (PEMECs) are structurally very versatile hybrid systems, combining the high solubilisable loading of microemulsions with the larger-scale structuring induced by the polymer, thereby markedly extending the concept of conventional PESCs. This type of system has not been described before and is highly promising for future applications where high payloads are to be formulated.

Received 10th September 2018

Accepted 15th October 2018

DOI: 10.1039/c8sc04013c

rsc.li/chemical-science

## Introduction

Microemulsions are thermodynamically stable liquid systems of water, oil and an amphiphile which are single-phase and optically isotropic<sup>1</sup> with structural properties that can be explained by the bending elasticity of their amphiphilic monolayers.<sup>2,3</sup> Frequent structural types are oil-in-water (O/W) droplets which naturally allow having a rather high content of hydrophobic material dispersed in aqueous solution, which otherwise could not be dissolved. From a fundamental point of view, O/W microemulsion droplets are interesting as they have a well-defined spherical structure and possess a low polydispersity when prepared close to the emulsification boundary.<sup>4</sup>

From a more practical point of view, microemulsions are an excellent medium for solubilising active agents, as often needed for formulations in cosmetics, pharmacy, *etc.*<sup>5–8</sup> However, in order to make them more versatile for such applications one may have to add additives like polymers to microemulsions which allow modulating their properties.

In a similar direction, polyelectrolyte/surfactant complexes (PESCs) have been studied comprehensively in the past few years. Because of their large structural variety,<sup>9–11</sup> that arises from the local structuring by the surfactant and the larger scale structuring by the polymer, they are considered to be very attractive for the purposes of solubilisation and drug delivery.<sup>12,13</sup> They have for instance been explored for the case of cationic hydrogels and sodium dodecyl sulfate (SDS), where controlled release of a hydrophobic drug was achieved and the loading capacity depended markedly on the charge density of the polymer.<sup>14</sup> Work regarding the solubilisation in PESCs was done for the case of SDS/TX-100 micelles complexed with poly(dimethylallylammonium chloride) (PDADMAC). This system showed an unchanged solubilisation power in the complexes compared to the initially present micelles.<sup>15</sup> Other studies regarding the solubilisation of hydrophobic compounds

<sup>a</sup>Stranski-Laboratorium für Physikalische und Theoretische Chemie, Institut für Chemie, Technische Universität Berlin, D-10623 Berlin, Germany. E-mail: miriam.simon@tu-berlin.de; michael.gradzielski@tu-berlin.de

<sup>b</sup>Institut Laue-Langevin, 38042 Grenoble, France

<sup>c</sup>Laboratoire Léon Brillouin (CEA-CNRS), Uni. Paris-Saclay, CEA-Saclay, 91191 Gif-sur-Yvette, France

† Electronic supplementary information (ESI) available. See DOI: 10.1039/c8sc04013c



within PESCs were concerned with the contaminant oil trichloroethylene (TCE). They confirmed such a solubilisation behaviour of PESCs and their use allowed for enhanced separation by using colloid-enhanced ultrafiltration processes.<sup>16</sup> Apart from that, PESCs of oppositely charged surfactant micelles and double hydrophilic polyelectrolytes have been investigated with respect to their ability to solubilize drug molecules, as for instance done for the case of the cationic copolymer poly(ethylene oxide)-*g*-polyethyleneimine (PEO-*g*-PEI) and sodium oleate.<sup>17</sup> Central for a successful application here is a high drug loading as was seen for doxorubicin (DOX) in PESCs obtained from combining poly(ethylene glycol)-*block*-poly(4-vinylbenzylphosphonate) (PEG-*b*-PVBP) with cationic surfactants.<sup>18</sup> In general it is important to optimise the ability to solubilise hydrophobic compounds, but typically the solubilisation capacity for drugs or dye molecules in PESCs is rather limited since only certain surfactants show high solubilisation capacities.<sup>19</sup>

Accordingly an interesting alternative is to use microemulsion droplets, which are structurally well understood and already contain a large amount of solubilised hydrophobic compounds,<sup>20</sup> and to complex them with oppositely charged polyelectrolytes, thereby forming polyelectrolyte/microemulsion complexes (PEMECs). This approach avoids the need for optimising the solubilisation properties as it is intrinsically controlled by the microemulsions. It is interesting to note that such mixtures so far have only been investigated very scarcely. In contrast, for instance the modification of microemulsion viscosity by polymeric additives has been studied in some detail and can be enhanced largely by adding hydrophobically modified telechelic water-soluble polymers, where the effect depends largely on the length of the hydrophobic modification and the amount of the added polymer.<sup>21–26</sup> Similarly complexes between neutral amphiphilic polymers and water-in-oil (W/O) microemulsions have been studied<sup>27</sup> and they can also be transformed into a transient network by ABA copolymers where the A blocks are hydrophilic.<sup>28</sup> The effect of polyelectrolytes on the phase behaviour and structure of W/O microemulsions was also studied, but mostly with the aim of forming nanoparticles in these systems.<sup>29,30</sup> Note *et al.* investigated the phase diagram of a negatively charged SDS/pentanol based W/O microemulsion with the cationic polyelectrolyte PEI<sup>31</sup> and found that more than 30 wt% PEI can be incorporated within the aqueous phase. The incorporation of PEI leads to a substantial shift of the microemulsion regime within the phase diagram, leading to the formation of bicontinuous and even O/W structures. In one of the few investigations on cationic surfactant–polyanion complexes, it was found that the solubilisation capacity of the micelles increases in the presence of the polymer, due to the additional ionic strength.<sup>32</sup> If charged droplets bind to polymers through electrostatic interactions, bridging and/or compactations of the droplets would be expected as well as a decoration of the polyelectrolyte chains with microemulsion droplets.<sup>33</sup> In general, the same structural richness is expected here, as seen for PESCs, while guaranteeing a high hydrophobic loading of the surfactant aggregates.

However, nearly no research has been carried out on mixtures of charged microemulsion droplets with oppositely charged polyelectrolytes, where the complexation would be driven by electrostatic interactions and concomitant counterion release and the idea of gaining structural control of the microemulsion system on a larger length scale *via* polyelectrolyte addition has not been exploited yet.

In order to fill this scientific gap, we investigated oil-in-water (O/W) microemulsion droplets based on tetradecyldimethylamine oxide (TDMAO), which is known to form such microemulsions with different alkanes.<sup>34</sup> The droplet size can be increased in a systematic fashion by addition of a cosurfactant, as has been demonstrated in detail in the case of 1-hexanol.<sup>35</sup> In addition, these microemulsion droplets can become variably charged without modifying their structure by substituting small amounts of TDMAO with the equivalent cationic surfactant tetradecyltrimethylammonium bromide (TTAB).<sup>36–38</sup> Accordingly, these microemulsions are highly suited for a systematic investigation as they are at the same time a well-defined and monodisperse model colloid and attractive for potential applications. It might be noted that we stayed in the range of having small amounts of ionic surfactant as the microemulsion itself is in principle a nonionic one and we just introduced some charges to allow for ionic assembly. As a simple oppositely charged polyelectrolyte we chose the sodium salt of the flexible polyacrylic acid (PAA), sodium polyacrylate (NaPA).

In the present experiments we varied the mixing ratio of microemulsion and NaPA, the radius of the droplets and the molecular weight of the NaPA, with the aim to deduce systematic correlations between these parameters, the phase behaviour and the formed structures. We also studied the effect of the total concentration on the formed structures, as well as a variation of ionic strengths in order to modify the electrostatic interactions in these systems. For the structural characterisation, we employed static and dynamic light scattering, measurements of the  $\zeta$ -potential, and small-angle neutron scattering (SANS). With the systematic variation of all relevant system parameters, we were able to gain a comprehensive insight into the structural arrangements at the mesoscopic scale as a function of these parameters (since access to the structure and dynamics of self-assembled systems is the key for their understanding<sup>39</sup>). The combination of these experimental methods shows that the formed polyelectrolyte/microemulsion complexes (PEMECs) are rich in their morphology and controlled by their composition and the details of the polyelectrolyte and microemulsion droplet employed.

## Results and discussion

### Sample preparation

Unless stated otherwise, the oil-in-water (O/W) microemulsion droplets were prepared from a 100 mM stock solution of surfactant where always 5 mol% of zwitterionic TDMAO was substituted by cationic TTAB to obtain weakly charged droplets while keeping the total surfactant concentration constant. Different droplet sizes were achieved by adding different amounts of the cosurfactant hexanol (0, 50 and 75 mM)<sup>35</sup> and



saturating the mixture with decane (30, 80 and 200 mM, respectively), which resulted in droplet radii of 3.1, 4.3, and 6.4 nm (named ME00, ME50 and ME75, respectively).

Different amounts of sodium polyacrylate (NaPA) were added to the microemulsion in order to vary the charge ratio  $z = [-]/[+] + [-]$  of the polyelectrolyte/microemulsion complexes (PEMECs) (it might be noted that here we refer to nominal charges, *i.e.* ionised or ionisable groups ( $-\text{NMe}_3$  and  $-\text{COOH}$ ), and not actual charges, which for the NaPA and TDMAO depends on the pH and chemical surrounding). The pH was checked after preparation but not further modified in order not to add additional ions to the sample. All samples had pH-values between 7 and 8, where the polyacrylate is about 90% ionised (see Fig. S1†) and TDMAO is only little protonated.

Most samples were prepared from microemulsion and polyacrylate stock solutions, which were then mixed in the desired ratios. However, the same results (complex size and shape) were obtained by mixing all 'dry' compounds (TDMAO, TTAB, hexanol, decane, and NaPA) first and adding water afterwards (see Fig. S2† for SANS curves of such an example), so we can safely assume that the observed structures are in thermodynamic equilibrium as they don't depend on the sample history.

### Phase behaviour

The determination of the macroscopic phase behaviour is very important since systems of oppositely charged colloids and polyelectrolytes have a tendency to phase separate at the vicinity of charge neutralisation.<sup>9,10</sup> This situation is complicated by the fact that this phase separation often occurs very slowly and careful investigation over a period of many days or weeks may be required in order to determine the equilibrium phase diagram.

Mixtures of cationic O/W TDMAO/TTAB/decane microemulsion droplets with negatively charged polyacrylate (NaPA) were studied at a fixed surfactant concentration of 100 mM (5 mM cationic TTAB + 95 mM uncharged TDMAO) and different amounts of NaPA to obtain different mixing ratios. In order to gain a comprehensive overview over the phase

behaviour, samples were prepared with different microemulsion droplet sizes and different chain lengths of the NaPA. A wide range of precipitation is observed around equimolar charge mixing ( $z \sim 0.5$ ) and only for the microemulsion or polyelectrolyte excess single phases are found. It is interesting to note that the biphasic region of the phase diagram has a very asymmetric shape, *i.e.* a polyelectrolyte excess provides much higher colloidal stability to the systems.

Samples close to the charge equilibrium ( $z = 0.5$ ) phase separate directly after mixing while samples away from  $z = 0.5$ , especially at microemulsion excess, appear turbid at first and need hours or even days for macroscopic phase separation, see Fig. 1. Samples that show phase separation in less than an hour after mixing were labelled biphasic. Metastable samples are samples which need from one hour up to one week to phase separate. Directly after mixing, the metastable samples appeared clear, but then changed colour to bluish and eventually white, before phase separating into a clear liquid and a solid, white precipitate. All samples that still consist of one single phase after one week were considered as thermodynamically stable single phase systems, as they did not evolve during the course of several months (examples of such samples can be seen in Fig. S3†).

It was observed that larger droplets and increasing  $M_w$  of the NaPA both lead to a larger biphasic region in the phase diagram. This increase is mostly visible at small  $z$ -values (microemulsion excess), where the phase boundary is strongly affected, inducing a much more pronounced precipitation with increasing  $M_w$  of NaPA and microemulsion droplet size. In contrast, the behaviour of the phase boundary for large  $z$  (polyelectrolyte excess) is basically independent of the  $M_w$  of the NaPA (Fig. 1). Immediate phase separation was observed to take place much more likely for the case of large droplets, which indicates a substantially lower kinetic stability of their complexes. It occurs already for the shortest NaPA (for which the small 3.1 nm droplets show rather slow precipitation and the metastability allowed investigating the structures over the whole  $z$ -range by light and neutron scattering experiments). This means that the phase behaviour depends strongly on the precise composition of the PEMEC systems.



Fig. 1 Phase diagrams showing the biphasic and the metastable regions for ME00 ( $R = 3.1$  nm), ME50 ( $R = 4.3$  nm) and ME75 ( $R = 6.4$  nm) at  $c$  (surfactant) = 100 mM, mixed with NaPA of different molecular weights and at different charge ratios  $z$ .



For long time stable single phase regions for smaller or larger  $z$ , the samples show different optical appearances ranging from clear to bluish (when being closer to the precipitation area), which indicates the formation of differently sized complexes as a function of  $z$  (see Fig. S3†). The formation of mixed aggregates was confirmed by the values of the  $\zeta$ -potential that reverses sign upon the addition of the NaPA (Fig. 2). What is also interesting to note here is that the  $\zeta$ -potential is reduced very abruptly upon the addition of NaPA.

### Structural characterisation of stable polyelectrolyte/microemulsion complexes (PEMECs)

The study of the phase diagrams has enabled the identification of single-phase regions of the NaPA/ME mixtures, which are either stable or at least long-time metastable. We were now interested to determine how the colloidal structure of these PEMECs depends on their molecular composition.

The optical appearance of the samples and the  $\zeta$ -potential values suggest that differently sized mixed aggregates are formed, which was confirmed by static and dynamic light scattering (SLS and DLS). Since light scattering (both static and dynamic) does not allow deducing mesoscopic structural information, small-angle neutron scattering (SANS) was used to access a refined mesoscopic structural picture. In all these

experiments, we systematically varied the mixing ratio of NaPA to ME charges, the molecular weight  $M_w$  of the NaPA and the size of the droplets, thereby gaining an insight into how the structure of the PEMECs can be controlled by their composition.

**Variation of the mixing ratio.** SLS and DLS studies were carried out with a series where at least metastable homogeneous samples are obtained for all mixing ratios, *i.e.* small microemulsion droplets ( $R = 3.1$  nm, Fig. 1 left) with a degree of charging of 5 mol% and increasing amounts of added NaPA with  $M_w = 5.1$  kg mol<sup>-1</sup>, while the concentration of the surfactant (and therefore that of O/W microemulsion droplets) was kept constant at 100 mM. The molecular weight of the formed complexes obtained from SLS (Fig. 3A) and also the hydrodynamic radii deduced from DLS (Fig. 3B) show that the size of the aggregates increases upon addition of the polyelectrolyte until a maximum is reached close to the charge equilibrium. With increasing polyelectrolyte excess, the aggregates become smaller again. It should be noted here that for this series the hydrodynamic radii obtained by DLS are relatively small about 1–7 nm (these aggregates become much bigger for longer NaPA as discussed in the ‘Variation of the NaPA Chain Length’ and see *e.g.* Fig. S4†). For small  $z$ -ratios, at microemulsion excess, the given DLS values are actually smaller than the real size, as DLS measures the collective diffusion coefficient, which is largely influenced by the repulsive interactions within the sample. For obtaining a correct  $R_h$  value the collective diffusion coefficient would have to be corrected with the structure factor (for instance obtained from the SANS measurements) according to:  $D_{\text{coll}}(q) = D_0/S(q)$ . For example, for pure ME00 the measured diffusion coefficient is 143  $\mu\text{m}^2 \text{s}^{-1}$  and  $S(0) = 0.3$  (deduced from SANS) thereby leading to a  $D_0$  value of 43  $\mu\text{m}^2 \text{s}^{-1}$  and a hydrodynamic radius of 5.6 nm. For polyelectrolyte excess, where aggregation occurs, the measured  $R_h$  has to be reinterpreted as well, since, according to the SANS data (Fig. 4A), the formed aggregates are not spherical but elongated. The measured  $R_h$  can be converted into the length of a rod  $L$  (with fixed diameter  $d$ ):  $\frac{kT}{6\pi\eta R_h} = D_t = \frac{kT(\ln p + C_t)}{3\pi\eta L}$  with  $p = L/d$  and  $C_t = 0.312 + 0.565/p - 0.100/p^2$ .<sup>40</sup> For example a measured diffusion coefficient of 34.2  $\mu\text{m}^2 \text{s}^{-1}$  (ME00–NaPA05,  $z = 0.7$ ) equals an  $R_h$  of 7 nm and corresponds to a rod



Fig. 2  $\zeta$ -Potential of microemulsion–polyelectrolyte complexes at different charge ratios, showing the transition from positively charged microemulsion droplets to negatively charged complexes. The metastable region is shaded in red.



Fig. 3 Apparent  $M_w$  and  $R_h$  obtained from static and dynamic light scattering show the presence of differently sized aggregates of ME and PE depending on the charge ratio  $z$ . Metastable samples (shaded in red) were measured while still being homogeneous, typically being 3–5 days old. Measured values for longer NaPAs are given in Fig. S4.†



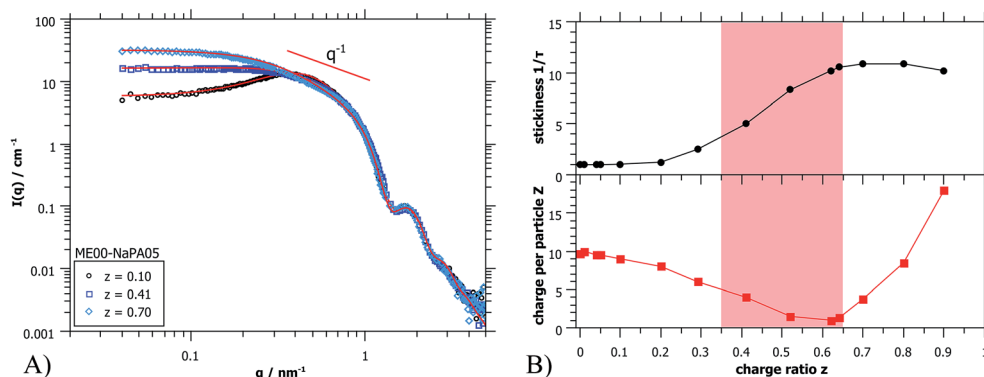


Fig. 4 (A) Fitted SANS spectra (PAXY at LLB) of three ME00–NaPA05 samples, showing the good agreement of the chosen structure factor model with the measured data points (fit curves as solid red lines). (B) Fit parameters ‘stickiness’  $1/\tau$  and ‘charge per particle’  $Z$  obtained from fitting the structure factor in dependence of the charge ratio  $z$ . The metastable region is shaded in red.

of 3 nm radius (one ME droplet) and 27 nm length (4.3 densely arranged droplets).

To complete the structural information gained from light scattering, additional SANS data were obtained. In Fig. 4A some selected SANS spectra for the same sample series are shown. The whole series is displayed in Fig. S5.† A very important finding is that the scattering curves for different charge ratios do not change at high  $q$  ( $q > 0.8 \text{ nm}^{-1}$ ), thereby indicating that in this size range ( $d < 8 \text{ nm}$ ), that characterizes the microemulsion droplets, the structure remains unchanged. It might be noted that this finding is valid in general for all systems investigated here, so the size, shape and polydispersity of the initially present microemulsion droplets are not affected by the addition of an oppositely charged polyelectrolyte. This is very important as it means that the microemulsion droplets remain structurally intact and would for instance be available as carriers in delivery systems.

The main difference in scattering intensity is seen at low  $q$  ( $q < 0.3 \text{ nm}^{-1}$ ), where the structure factor describes the interactions between the particles. This indicates that at small amounts of NaPA the charge of the ME droplets is screened and one observes a continuous increase of intensity with increasing content of NaPA ( $z = 0.0 - 0.5$ ). Once all ME charges are screened, the PE starts to introduce attractive interactions, which increases the intensity even further. For high NaPA excess ( $z > 0.6$ ) the intensity starts to decrease somewhat with increasing  $z$ , indicating a collapse of the structures, probably due to the large excess of negative charge and the resulting strong electrostatic repulsion between aggregates contained.

For quantitative analysis of the SANS curves the intensity  $I(q)$  was approximated as:

$$I(q) = {}^1N V^2 \Delta \text{SLD}^2 P(q) S(q) \quad (1)$$

where  ${}^1N$  is the number density of scattering particles,  $V$  the volume of the particles,  $\Delta \text{SLD}$  the contrast between aggregates and solvent (Table S1†),  $P(q)$  the hard sphere form factor (with a LogNormal size distribution) and  $S(q)$  the structure factor (experimental smearing was accounted for as described in (ref. 41) and the ESI†). The chosen model for  $S(q)$  for this series was

that of sticky hard spheres in Percus–Yevick approximation (Baxter model<sup>42</sup>) into which an electrostatic repulsion<sup>43</sup> was incorporated *via* random phase approximation (RPA) as previously done for ideal hard spheres.<sup>44</sup> In this fashion the structure factor accounts at the same time for the electrostatic repulsion between the equally charged microemulsion droplets and for the effective attractive interaction between the droplets that become bridged by the NaPA eqn (S4)–(S7) (ESI†). This model allows determining an effective charge per particle and the stickiness parameter  $1/\tau$ . The values are summarized in Fig. 4B and Table S2.† It can be seen that the deduced charge per particle decreases with increasing complexation by the NaPA within the surfactant excess region, but then increases again in the NaPA excess region. This may be explained partly by an overcharging due to the binding of the NaPA. It may also be explained by the increasing amount of NaPA chains that introduce steric and electrostatic repulsion. In our model (where the steric part arising from the excluded volume of the droplets is kept constant) the increase of charge can only be compensated by a larger charge, as it is the effective repulsive parameter. The stickiness parameter  $1/\tau$  is small but increases in the surfactant excess region and then becomes much larger in the NaPA excess regime, which indicates that here the droplet bridging is most effective.

This model works very well for small droplets and short PE chains. But only attractive and repulsive forces are not enough to describe the more elongated complexes as they are formed by higher  $M_w$  polyacrylates (see the ‘Variation of the NaPA Chain Length’).

**Variation of the microemulsion droplet size.** The previous measurements were done with small droplets of 3.1 nm hydrodynamic radius but complexes can also be formed with larger droplets of 4.3 and 6.4 nm, as already shown in the phase diagrams. The droplet size has no effect on their structural integrity during the complexation with NaPA, as seen in SANS (see Fig. S6†). However, the average number of charged surfactants in them varies substantially being 12.1, 23.2 and 51.5 respectively, with increasing size.

SLS measurements of samples with differently sized droplets but mixed with the same NaPA at the same charge ratio



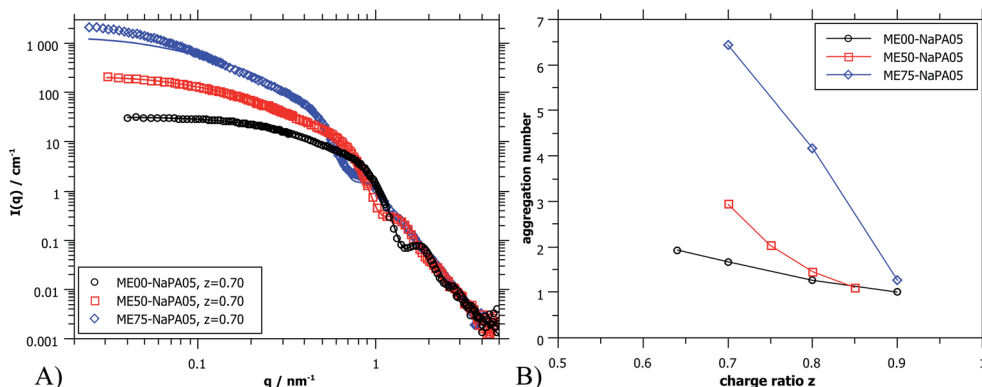


Fig. 5 (A) SANS scattering curves (ME00 and ME50 from PAXY at LLB and ME75 from D11 at ILL) of complexes formed with differently sized microemulsion droplets and NaPA05. Solid lines were calculated for a cylindrical arrangement of the droplets.<sup>45</sup> (B) Aggregation number  $N_{\text{agg}}$  of ME droplets contained in the aggregates as deduced from extrapolated  $I(0)$  values of SANS curves (for details see the ESI†).

naturally show a much higher intensity for bigger droplets, *i.e.* higher  $M_w$  complexes are formed, reaching values of  $10^6 \text{ g mol}^{-1}$  (it might also be noted that the hydrodynamic radius, measured with DLS, increases by a factor of 2.5, reaching values of 25 nm, see Fig. 6).

Again, further insight can be obtained from SANS measurements carried out at different mixing ratios  $z$  with all droplet sizes; the curves are shown in Fig. S6.† All series show the same general behaviour regardless of the droplet size, but the intensity extrapolated to  $q = 0$ ,  $I(0)$  (or equivalently the  $M_w$  of the complexes) increases strongly with increasing droplet size (see Fig. 5A, S7 and S8†). The number of microemulsion droplets contained in one complex was obtained from the scattering at zero angle,  $I(0)$  (obtained by extrapolation with Guinier approximation), compared to the forward scattering of a single non-interacting microemulsion droplet. This analysis is described in detail in the ESI† and results are shown in Fig. 5B. Here it was assumed that the contribution of the polyelectrolyte to the scattering intensity can be neglected in comparison to the scattering of the microemulsion droplets. This approach is only meaningful for polyelectrolyte excess as for microemulsion excess one just sees a modification of the interaction potential from which no aggregation number can be deduced. At polyelectrolyte excess, the highest aggregation numbers are found close to the phase boundary. Only 2 of the small droplets seem

to be effectively linked in one aggregate but this number increases to 3 and even 6 of the medium and large droplets. The corresponding number of NaPA chains per complex can be calculated as follows:

$$\frac{N_{\text{chains}}}{\text{complex}} = \frac{[\text{NaPA}]}{[\text{ME}]} N_{\text{agg}} = \frac{N_{\text{TTAB}}}{\text{DP}} \frac{z}{1-z} N_{\text{agg}} \quad (2)$$

where  $N_{\text{TTAB}}$  is the average number of TTAB molecules per droplet (see Table 1), DP is the average degree of polymerization and  $N_{\text{agg}}$  is the number of ME droplets per complex as obtained from Guinier approximation. The results are summarised in Table 2.

At first glance the results look counterintuitive, as for the small droplets this corresponds to a situation where only one NaPA is involved in the complex. This number then increases to  $\sim 14$  NaPA chains in one complex for the largest droplets (ME75). This increase can be explained by the higher number of

Table 1 Structural parameters of pure microemulsion droplets

| Name | $c/\text{mM}$<br>(TDMAO/TTAB) | $c/\text{mM}$<br>(hexanol) | $c/\text{mM}$<br>(decane) | $R/\text{nm}$<br>(SANS) | [+]/droplet |
|------|-------------------------------|----------------------------|---------------------------|-------------------------|-------------|
| ME00 | 95/5                          | 0                          | 30                        | 3.1                     | 12.1        |
| ME50 | 95/5                          | 50                         | 80                        | 4.3                     | 23.2        |
| ME75 | 95/5                          | 75                         | 200                       | 6.4                     | 51.5        |

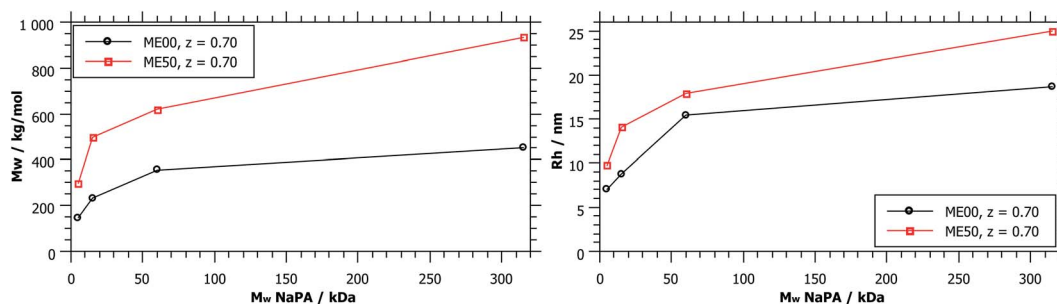


Fig. 6  $M_w$  and  $R_h$  obtained from static and dynamic light scattering as a function of  $M_w$  (NaPA), comparing different droplet sizes for a charge ratio  $z = 0.7$ .  $M_w$  (ME00) =  $52 \text{ kg mol}^{-1}$  and  $M_w$  (ME50) =  $110 \text{ kg mol}^{-1}$ .



Table 2 Structural parameters of different PEMECs from Guinier analysis

| ME   | NaPA | $z$ | $N_{\text{droplets/complex}}$ | $N_{\text{chains/complex}}$ | Comment                                 |
|------|------|-----|-------------------------------|-----------------------------|---|
| ME00 | 5.1  | 0.7 | 1.7                           | 1                           | Stiff rod                               |
|      | 15   | 0.7 | 2.6                           | 0.5                         | Stiff rod                               |
|      | 60   | 0.7 | 8.8                           | 0.4                         | Rod starts to bend                      |
|      | 315  | 0.7 | 15.7                          | 0.2                         | Exact number of droplets not detectable |
| ME50 | 5.1  | 0.7 | 2.9                           | 3                           | Stiff rod                               |
|      | 15   | 0.7 | 3.5                           | 1.2                         | Rod starts to bend                      |
|      | 60   | 0.7 | 12.6                          | 1                           | Exact number of droplets not detectable |
|      | 315  | 0.7 | 22.9                          | 0.5                         | Exact number of droplets not detectable |
| ME75 | 5.1  | 0.7 | 6.4                           | 14                          | Rod starts to bend                      |

charges per droplet, which increases with increasing droplet size, and allows for a much more effective electrostatic polyelectrolyte/droplet interaction. At higher mixing ratios ( $z = 0.9$ ), the NaPA excess is high enough to stabilize each droplet separately, regardless of the size, so the value of  $N_{\text{agg}}$  drops to 1. In general, this is a relatively low number of aggregated microemulsion droplets compared to the typical aggregation number observed in PESCs, but it must also be noted that  $N_{\text{agg}}$  increases largely with increasing  $M_w$  of the NaPA (see the 'Variation of the NaPA Chain Length').

The most elongated complexes are present close to the phase boundary. SANS curves at  $z = 0.7$  (Fig. 5A and further curves are shown in S6†) were described by a model of spheres arranged in a cylindrical domain as described in (ref. 45) (for further details also see the ESI†). This model describes more correctly the low  $q$ -range of the curves as the sticky hard sphere model since it accounts more correctly for the local shape of the aggregates. Here the elongation becomes clearly more pronounced with increasing size of the microemulsion droplets.

**Variation of the NaPA chain length.** As illustrated in Fig. 4, SANS curves show a pronounced  $q^{-1}$  behaviour in the low  $q$ -range. This is observed mainly for samples close to the phase boundary, indicating locally rod-like structures. The experiments discussed so far were all done with the shortest NaPA of  $M_w = 5.1 \text{ kg mol}^{-1}$ . The stretched chain of this polyelectrolyte is about 14 nm long, so effectively only two microemulsion

droplets can be linked by one polyelectrolyte chain. As a next parameter variation, we increased the length of the NaPA chain to induce the formation of more elongated structures.

As shown in Fig. 1, complexes formed with longer NaPA chains have a larger two-phase region. For the stable samples in the range of NaPA excess SLS shows a significant increase of the molecular weight of the formed aggregates with increasing  $M_w$  of the NaPA (Fig. 6). Simultaneously the hydrodynamic radius determined by DLS substantially increases, for instance for the ME00 system rising from about 7 to almost 20 nm when increasing the  $M_w$  of the NaPA from 5.1 to 315  $\text{kg mol}^{-1}$ . The growth of PEMECs is confirmed by  $I(0)$  from SANS (Fig. S7 and S8†). It is also shown that this is a generic observation, which is valid for all droplet sizes.

The static light scattering at  $I(0)$  shows the formation of complexes of higher  $M_w$  but does not give further information regarding their structure. If a rod with a diameter of the droplet size was assumed, a measured diffusion coefficient of  $15.6 \mu\text{m}^2 \text{ s}^{-1}$  (ME00–NaPA60,  $z = 0.7$ ) would equal a length of 95 nm (15 densely arranged droplets). More information about the exact shape of the formed aggregates can be obtained from SANS measurements. A direct comparison of the SANS curves at a given mixing ratio  $z$  ( $z = 0.7$ ) and for identically sized microemulsion droplets (Fig. 7A) shows that with increasing  $M_w$  of the NaPA the SANS intensity at low  $q$  increases and shows a more pronounced linear part, which follows a  $q^{-1}$  law, thereby

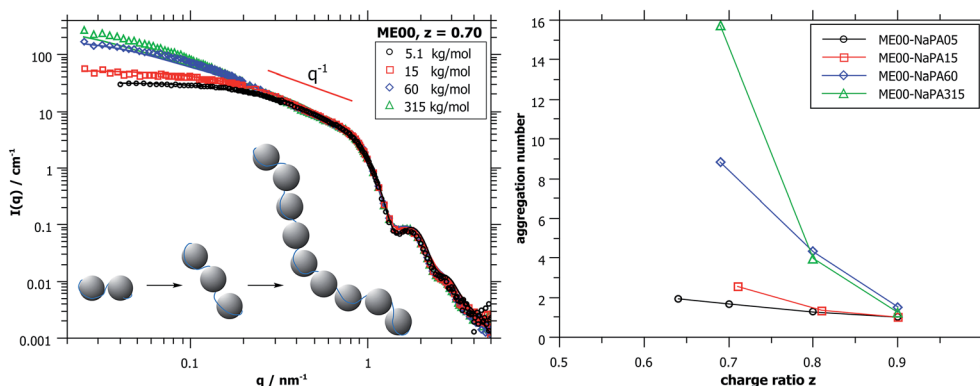


Fig. 7 (A) Comparison of complexes formed with ME00 and NaPA of different  $M_w$  at a charge ratio  $z = 0.7$  in the polyelectrolyte excess, where the biggest complexes are formed (NaPA05 and 15 from PAXY at LLB and NaPA60 and 315 from V4 at HZB). Solid lines were calculated for a cylindrical arrangement of the droplets. (B) Aggregation number  $N_{\text{agg}}$  deduced from extrapolated  $I(0)$  values of SANS data, compared for different NaPA chain lengths.



indicating the formation of increasingly more elongated complexes. The elongation of these complexes close to the phase boundary becomes more pronounced when a longer NaPA chain is employed.

One possible explanation for forming elongated complexes would be the transformation of many droplets into a cylinder with a diameter of one droplet. However, as mentioned before, the form factor minimum does not change, so the size and shape of the microemulsion droplets remain the same. Another way to form elongated complexes is by linking several droplets with polyelectrolyte chains in a cylindrical geometry. A comparison of the two models is given in Fig. S9,<sup>†</sup> showing the significantly better agreement of the second model with the measured data. Accordingly, this model was used to describe the SANS data and to quantify the elongation. The structural parameters for single microemulsion droplets were fixed to be those of the pure microemulsion sample. Additional parameters for the linear arrangement of the droplets are the number  $N$  of droplets per aggregate, the mean distance  $D$  between droplets in one aggregate and the polydispersity of this distance.

It has to be mentioned here that this model describes the measured data for short chains but the agreement becomes poorer with longer polyacrylate chains. This can be explained by the flexible nature of the polyacrylate backbone. In the model the droplets arrange to form a straight, stiff rod, which gives a slope of  $q^{-1}$  in the SANS data. In practice, however, longer aggregates composed of many droplets will tend to be less straight, which finally would lead to a slope of  $q^{-2}$  for Gaussian coils. The longest polyacrylate chain employed in this work has an  $M_w$  of 315 kDa with a stretched chain length of about 850 nm. This polyelectrolyte does not form straight rod-like complexes over the whole length scale but bends over its persistence length, and therefore the SANS data show a slope of  $q^{-1.5}$ .

The curves shown in Fig. 7A were described with cylindrical arrangements of 1.5, 3, 11 and 17 droplets per aggregate for  $M_w$ s of the NaPA of 5.1, 15, 60 and 315 kDa, respectively.<sup>45</sup> The model-results for the longest NaPA (315 kDa) are not reliable anymore but here a number of 16 droplets per aggregate can be obtained from the  $I(0)$  value of the scattering data. More results obtained from the fits, also for larger droplets, are given in

Table S3,<sup>†</sup> while the aggregation numbers obtained from the forward scattering  $I(0)$  are given in Fig. 7B and Table 2.

**Concentration of the complexes.** Another parameter of interest is the total concentration. In order to address this point we investigated a concentration series of complexes of ME00 (smallest droplets with no added hexanol, because hexanol is partly water soluble, thereby complicating the dilution procedure) and 15 kg mol<sup>-1</sup> NaPA, prepared at 600 mM surfactant concentration and diluted down to 10 mM. It was observed that the colloidal stability mainly depends on the mixing ratio  $z$  and the  $M_w$  of the NaPA but not on the overall concentration. The samples stayed visually clear when diluted and no phase separation was observed. Selected SANS patterns for the microemulsion excess region ( $z = 0.1$ ) are shown in Fig. 8 (full set of data in Fig. S10<sup>†</sup>). They are normalized for the concentration (divided by the volume fraction of droplets,  $\phi$ ) and show nicely that upon dilution of the system the microemulsion correlation peak moves as expected to lower  $q$  (larger spacing). It is important to note here that the form factor minimum, which shows the droplet size, is at the same position for all concentrations. We can therefore assume that the spherical microemulsion droplets are still present down to surfactant concentrations of 10 mM and no bigger emulsion droplets have formed. However, at low concentration (below 100 mM of surfactant) one also observes a pronounced increase of the scattering intensity at low  $q$ . This can be attributed to the fact that at higher concentration the NaPA is able to bridge the microemulsion droplets yielding a space-filling network. However, once diluted too much this is no longer possible and now this network dissolves, thereby forming relatively large clusters that are scattering more strongly at low  $q$ .

The forward scattering intensities were obtained by Guinier approximation. The results are shown in Fig. 8B and it can be seen that this increase is much more marked on the side of microemulsion excess. Here one may argue that one observes a transition from a space-filling polyelectrolyte/microemulsion network at higher concentration to increasingly isolated clusters due to diluting below the effective overlap concentration. For  $z = 0.7$  a gradual increase of  $I(0)$  is observed. Because of the much higher starting concentration of NaPA no concentrations below

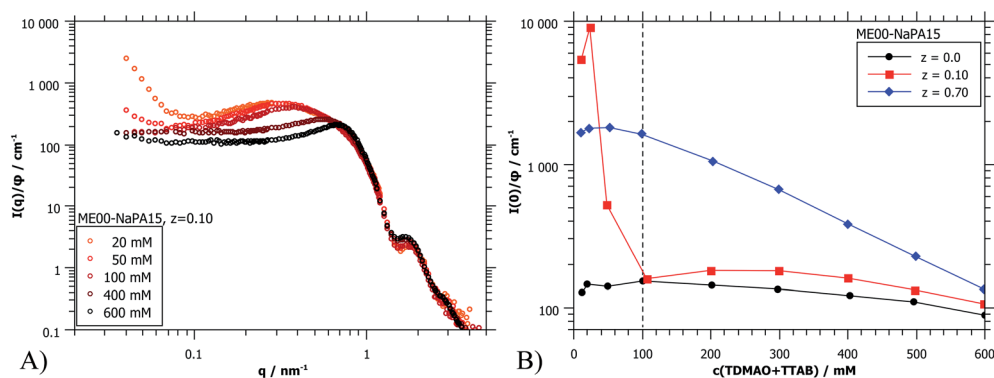


Fig. 8 (A) Selected SANS curves (PAXY at LLB) of the dilution series of ME00–NaPA15 complexes, normalized by volume fraction  $\phi$ . (B)  $I(0)/\phi$  for three different charge ratios; the charge ratios were chosen to be below and above the two phase region of the phase diagram. The dotted line shows the concentration of all other samples presented in this work.





the effective overlap concentration are reached. But below 100 mM no further changes of the scattering curves are seen upon still diluting further (Fig. 8B and S10†). Apparently here the system is diluted enough that individual complexes are visible.

**Effect of ionic strength – addition of salt.** Since the complexes examined in this study are always based on electrostatic interactions, it is interesting to investigate their behaviour at different ionic strengths. This was done by adding different amounts of sodium chloride to already formed complexes. Fig. 9A shows SANS curves at two different charge ratios of  $z = 0.1$  and  $0.7$  with added salt (50 mM) compared to the same samples without salt. The scattering curves show clearly that the repulsive interaction of the charged microemulsion droplets is strongly reduced (almost extinguished) as well as the attractive interaction of the complexes. This can be seen in the increased or decreased scattering at low  $q$  for the repulsive and attractive interaction, respectively. Complementary SANS curves for different amounts of added salt are given in Fig. S11.†

Fig. 9B shows  $I(0)$  as a function of ionic strength which modifies the interactions between the droplets. For the case of  $z = 0.1$  (microemulsion excess) the added salt apparently screens the charges of the microemulsion droplets already effectively for less than 20 mM NaCl. This is the expected behaviour for such systems as here the spacing between the droplets becomes much larger than the Debye screening length  $\delta$  (for 20 mM ionic strength:  $\delta = 2.3$  nm).<sup>36</sup> However, the behaviour of polyelectrolyte excess is surprising since a concentration of 50 mM seems to be sufficient to dissolve the PEMECs that are held together by electrostatic interactions. This is in striking contrast to observations for polyelectrolyte/surfactant complexes (PESCs) or interpolyelectrolyte complexes (IPECs), where typically an ionic strength of 500–700 mM is required in order to dissolve them.<sup>46–48</sup> Apparently the PEMECs studied here possess a very high degree of responsiveness to ionic strength.

## Discussion

These experimental observations can be interpreted in terms of molecular build-up of the studied PEMECs. The main parameters to be considered are:

- The length of the polyelectrolyte and its charge density.
- The size of the microemulsion droplets (controlled by the amount of 1-hexanol contained) and the number of charges (TTAB content) on them.
- Their mixing ratio as defined by  $z = [-]/([-] + [+])$ .
- The ionic strength of the solution.

When looking at the present PEMECs it is clear that especially the overlap concentration of the different NaPAs employed varies largely and therefore also their ability to build a space-filling polyelectrolyte network. On the other hand the microemulsion droplets have a rather low number of charges, with about one charge per 12 nm<sup>2</sup>, while the charge density along the NaPA backbone is rather high, with one charged unit per 0.25 nm (this situation is depicted in Fig. 10A). This makes their interaction delicate explaining why the larger droplets have a higher tendency for precipitating as here simply the number of charges per droplet is higher and therefore it allows more easily compensating for the high charge density of the NaPA (this even more so as they are curved less, thereby making it easier for the NaPA to bend around the microemulsion droplets).

Complexes with longer NaPAs (60 and 315 kg mol<sup>-1</sup>) prepared at polyelectrolyte excess ( $z > 0.5$ ) are already above the overlap concentration of the polyelectrolyte (calculated for a stretched chain). So, a network of polyelectrolyte chains is formed in the solution if no microemulsion droplets are present. Adding the oppositely charged microemulsion droplets deforms the network so that the droplets are arranged in one-dimensional complexes, which are held together by several NaPA chains (see Fig. 10B). Effective charge compensation by just one single NaPA chain is entropically unlikely. The extension of this cylindrical structure becomes larger with increasing  $M_w$  of the NaPA, as one may expect for longer chains. Therefore the length of one complex increases with increasing length of the NaPA chain, but only to a limited extent as the negative charge density of the complexes rapidly increases due to the fact that the charge density of the NaPA is much higher than that of the microemulsion droplets. This effect is influenced by the size of the droplets as with increasing size the local amount of positive charges increases and therefore the possibility of building larger aggregates becomes electrostatically enhanced.

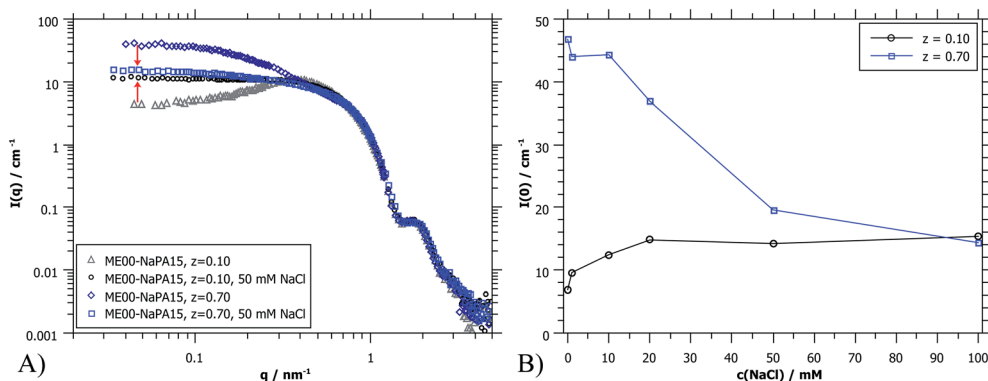


Fig. 9 (A) SANS curves (PAXY at LLB) of ME00–NaPA15 samples at two  $z$ -ratios (just below and just above the two phase region) before and after addition of 50 mM NaCl. (B)  $I(0)$  as obtained from SANS for the same samples with different amounts of NaCl added.





Fig. 10 Sketch of the structural arrangement in the TDMAO/TTAB/decane – NaPA polyelectrolyte/microemulsion complexes (PEMECs). (A) Single chain decorated NaPA chains (situation of ME excess) and zoom to the decoration of a droplet (drawn to scale for droplets with  $R = 3.1$  nm); (B) network with elongated complexes (situation with polyelectrolyte excess); (C) cluster with compacted ME droplets (situation with polyelectrolyte excess and high dilution).

This then explains the experimentally observed elongation of the complexes with increasing droplet size.

The behaviour is also interesting as a function of concentration. By dilution one will reach a critical concentration below the overlap concentration and therefore a network is no longer formed. For the case of polyelectrolyte excess, in the simplest case this then leads to a situation where a single NaPA chain will form a cluster which then contains the number of microemulsion droplets ( $[ME]/[PA]$ ) according to the stoichiometric composition (see Fig. 10C), which is given as:

$$\frac{[ME]}{[PA]} = \frac{DP}{N_{TTAB}} \frac{1-z}{z} \quad (3)$$

where DP is the average degree of polymerization and  $N_{TTAB}$  the average number of TTAB molecules per droplet (see Table 1). With this simple model we can calculate the expected number of microemulsion droplets per PE chain, which for the ME00 ( $R = 3.1$  nm,  $N_{TTAB} = 12.1$ ) droplet series just across the phase boundary ( $z = 0.70$ ) yields values of 1.9, 5.5, 22 and 115 for the 5.1, 15, 60 and 315 kDa NaPA, respectively. These values compare well with the data displayed in Fig. 9. For the longest NaPA chains the experimental values are still lower at the lowest experimental concentration, but they also still increase upon dilution in the light scattering experiment, as for the very long chains it is getting increasingly difficult to reach the dilute regime, where only single ME-decorated chains are still visible. Accordingly, under dilute conditions one really forms complexes that are based on a single PE chain as depicted in Fig. 10C.

Finally, the rather pronounced sensitivity of the complexes to the addition of salt can be discussed in the context of the driving force of complexation. For the case of counterion release by electrostatic binding of negative polyelectrolyte charges to the positive charges of the microemulsion droplets the driving force can be estimated by  $\Delta G_{com} = NkT \ln(V_2/V_1)$ .  $V_2$  is the volume available per counterion after complexation and  $V_1$  before complexation. However, the value of  $V_1$  for the droplets should be much larger than for an ionic surfactant micelle due to the much lower charge density on the droplet surface, in our case this charge density is only 5% (the droplets contain only 5 mol% of ionic surfactant). Accordingly, the volume ( $V_1$ ) available per ion should be about 20 times more than for a pure

micelle (the volume per ion will be given by the surface area times a layer thickness, which should be about the same for both cases and be less than the Bjerrum length).  $V_2$  is the volume in solution per free ion, which is inversely proportional to the total ion concentration in solution. Therefore in order that  $\Delta G_{com}$  becomes zero (and the driving force for complexation vanishes) if  $V_1$  is by a factor of 20 larger one may estimate that a correspondingly lower salt concentration is already effective in dissolving the complexes. This was observed experimentally in this work, as 20–50 mM of salt were enough to dissolve the PEMECs while for typical PESCes 500–700 mM of salt are needed.<sup>46–48</sup>

## Conclusions

In this work, for the first time, the complex formation between oppositely charged oil-in-water (O/W) microemulsion droplets and polyelectrolytes was systematically studied. The charge on the droplets was kept relatively low by only having 5% of the surfactant head groups charged. This allows forming hybrid systems (polyelectrolyte/microemulsion complexes: PEMECs) with highly loaded surfactant carriers in a simple way. To obtain a broad overview of the behaviour of this system, the charge ratio  $z$  between the microemulsion and polyelectrolyte (sodium polyacrylate, NaPA), the size of the microemulsion droplets, the NaPA chain length and the overall concentration were varied.

Phase diagrams showed that the region of stable complexes becomes smaller with increasing  $M_w$  of the NaPA and with increasing size of the microemulsion droplets, as the larger droplets can interact more effectively with the polyelectrolyte. Depending on the charge ratio  $z$  between the microemulsion and polyelectrolyte, differently sized and shaped complexes are formed as examined in detail with SANS measurements. In the microemulsion excess region and at high enough concentration the added NaPA simply interconnects microemulsion droplets and reduces their repulsive interactions. The binding to the droplets can be seen in the decreasing number of charges per droplet that was obtained from the structure factor and when diluting the sample below a critical concentration. As  $z$  increases further, the complexes quickly become unstable. The closer the charge ratio is to the charge equilibrium, the more



easily the samples precipitate as there is less excess charge for stabilisation.

In the polyelectrolyte excess region the complexes are negatively charged on the outside and therefore electrostatically stabilised. The biggest complexes were found close to the phase boundary and they become smaller with increasing polyelectrolyte excess (larger  $z$ ). In this region structural changes of the complexes were found. Close to the phase boundary, the complexes have a cylindrical shape and are more elongated with longer polyelectrolyte chains. At very high  $z$ -values, the NaPA excess is high enough to stabilize each droplet separately. The dependence of the complexes on  $z$  was similar for all tested droplet sizes and NaPA chain lengths. The effect was more pronounced for larger droplets, which lead to bigger complexes, as well as for longer NaPA chains. With longer NaPA chains it is possible to link more droplets, so more elongated aggregates are formed.

Upon dilution, one forms complexes of single PE chains decorated with a stoichiometric number of ME droplets, which means that the aggregation number of the effectively observed complexes increases upon dilution. What is also interesting is the high sensitivity of the complexes to salt addition. This can be explained by the rather low charge density of the ME droplets and the correspondingly reduced entropy gain by counterion release in the complexation process.

In summary it can be stated that the examined complexes of O/W microemulsion droplets with oppositely charged polyelectrolytes (PEMECs) are structurally very versatile hybrid systems, responsive to concentration and ionic strength. Many different properties in architecture and size are accessible by systematically tuning the composition. For instance the complex size increases by having longer NaPA chains and bigger ME droplets. Using a microemulsion instead of micelles makes PEMECs markedly superior to conventional PESCs as loaded colloidal carrier systems. This allows combining the high loading capacity of a microemulsion with mesoscopic structuring *via* polyelectrolyte complexation, thereby having the functionality of both components within a self-assembled hybrid system. Such systems are highly promising for future fundamental investigations and applications in which a high payload is to be formulated within a complex colloidal system, thereby advancing the field of colloid science into the area of controlling microemulsion properties by ionic assembly.

## Experimental section

### Materials

The surfactants used in the experiments were tetradecyldimethylamine oxide (TDMAO, received as a gift from Stepan company, USA, as a 25% TDMAO solution in water named Ammonyx M. The solution was freeze dried before use) and tetradecyldimethylammonium bromide (TTAB, 99%, Sigma Aldrich, used without further purification). 1-Hexanol (>98%, MERCK-Schuchardt OHG) was used as a cosurfactant and decane (>98%, Fluka Chemika) as oil to form the microemulsions.

The employed polyelectrolyte is the sodium salt of polyacrylic acid (PAA), *i.e.*, sodium polyacrylate (NaPA) which was either purchased directly or prepared by adding a stoichiometric amount of NaOH to the PAA. The molecular weights used in this work were: 5.1 kg mol<sup>-1</sup> (DP = average degree of polymerization  $[-]/\text{polymer} = 54$ ; sodium salt, used as obtained from Sigma Aldrich), 15 kg mol<sup>-1</sup> (DP = 160; sodium salt solution from Sigma Aldrich, freeze dried before use), 60 kg mol<sup>-1</sup> (DP = 638; sodium salt, used as obtained from Fluka Chemika) and 240 kg mol<sup>-1</sup> (PAA; solution from Acros Organics, prepared by adding a stoichiometric amount of NaOH to the solution and freeze dried before use, which results in an average molecular weight of 315 kg mol<sup>-1</sup> for NaPA, DP = 3330). These molecular weights correspond to the lengths of the stretched polyelectrolyte of 14, 40, 160, and 850 nm respectively. The corresponding overlap concentrations for these polymers (assuming fully stretched chains) are 32, 3.9, 0.25, and 0.007 mM (in monomer units).

All samples were prepared in Milli-Q water or D<sub>2</sub>O (>99.5% D, Eurisotop) for the SANS experiments.

### Methods

Static (SLS) and dynamic (DLS) light scattering measurements were performed simultaneously on an ALV/CGS-3 instrument, with a He-Ne laser with a wavelength of  $\lambda = 632.8$  nm. Pseudo-cross-correlation functions were recorded using an ALV 5000/E multiple- $\tau$  correlator at scattering angles  $\theta$  ranging from 40 to 130° set with an ALV-SP 125 goniometer. The SLS curves were recorded in the same range of the magnitude of the scattering vector ( $q$ ), with

$$q = \frac{4\pi n_0 \sin(\theta/2)}{\lambda} \quad (4)$$

where  $n_0$  is the refractive index of the solution and  $\theta$  the scattering angle. All measurements were carried out at  $25.0 \pm 0.1$  °C in a thermostated toluene bath.

Small angle neutron scattering (SANS) experiments were carried out on the PAXY instrument of the Laboratoire Léon Brillouin (LLB) in Saclay. Measurements were performed in three configurations with sample-to-detector distances of 1.2, 2, and 6 m, collimation lengths of 2, 2, and 6 m and wavelengths of 4, 10, and 10 Å, respectively, to cover a  $q$  range from 0.031 to 5.05 nm<sup>-1</sup>.

Some additional SANS measurements were performed on the V4 instrument at the Helmholtz Zentrum Berlin (HZB).<sup>49</sup> The samples were measured at wavelengths of 4.5, 4.5 and 10 Å with sample to detector distances of 1.35, 6.75 and 15.75 m and collimation length of 2, 8 and 16 m respectively.

Further measurements were performed on the D11 instrument at the Institut Laue-Langevin (ILL) in Grenoble.<sup>50,51</sup> The samples were measured at a wavelength of 6 Å with sample to detector distances of 1.5, 8 and 34 m and collimation lengths of 8, 8 and 34 m, respectively.

Data reduction for PAXY and V4 data was done using Ber-SANS software.<sup>52</sup> For the D11 data, LAMP software was used.<sup>53</sup> The raw intensity data were corrected for the scattering of the



background (solvent and sample containers) and weighted by the transmission of the sample. Additionally, the (electronic) background noise was subtracted using a cadmium sample, which absorbs all incoming neutrons. The normalization and absolute scaling were done by using a 1 mm reference sample of distilled water, as an isotropic scatterer. Finally, the 2D data were radially averaged in 1D scattered intensity.

The wavelength smearing of the PAXY and V4 data described by the corresponding resolution parameters was incorporated into the analysis using SASfit software.<sup>54</sup> The wavelength spread (FWHM) was 10% and the detector pixels were 5 × 5 mm for both instruments. For D11 measurements the wavelength smearing was included in the x-error. More details are given in the ESI.†

SANS fits were performed in absolute units and it was assumed that all of the surfactant, cosurfactant, and oil are contained in the aggregates. Due to the low concentration and its rather homogeneous distribution in the sample, the polyelectrolyte was not considered explicitly for modelling of the data. More information on the models used to describe the SANS data is given in the ESI.†

ζ-Potential measurements were performed using a Litesizer 500 (Anton Paar) at 25 °C and a wavelength of λ = 658 nm and with a laser power of 40 mW.

## Conflicts of interest

There are no conflicts to declare.

## Acknowledgements

We thank the Laboratoire Léon Brillouin (LLB), the Helmholtz-Zentrum Berlin (HZB) and the Institut Laue-Langevin (ILL) for allocated beamtimes. We also thank Sylvain Prévost for his support during the SANS beamtime at LLB and Uwe Keiderling for his support during the beamtime at HZB. M. Simon thanks the TU Berlin for funding her PhD project.

## Notes and references

- 1 I. Danielsson and B. Lindman, *Colloids Surf.*, 1981, **3**, 391–392.
- 2 P. G. De Gennes and C. Taupin, *J. Phys. Chem.*, 1982, **86**, 2294–2304.
- 3 M. Gradzielski, D. Langevin and B. Farago, *Phys. Rev. E*, 1996, **53**, 3900–3919.
- 4 S. H. Chen, *Annu. Rev. Phys. Chem.*, 1986, **37**, 351–399.
- 5 P. P. Constantinides, *Pharm. Res.*, 1995, **12**, 1561–1571.
- 6 J. Lu, P. J. Liyanage, S. Solairaj, S. Adkins, G. P. Arachchilage, D. H. Kim, C. Britton, U. Weerasooriya and G. A. Pope, *J. Pet. Sci. Eng.*, 2014, **120**, 94–101.
- 7 J. Henle, P. Simon, A. Frenzel, S. Scholz and S. Kaskel, *Chem. Mater.*, 2007, **19**, 366–373.
- 8 P. Boonme, *J. Cosmet. Dermatol.*, 2007, **6**, 223–228.
- 9 L. Chiappisi, I. Hoffmann and M. Gradzielski, *Soft Matter*, 2013, **9**, 3896–3909.
- 10 D. Langevin, *Adv. Colloid Interface Sci.*, 2009, **147–148**, 170–177.
- 11 M. Rinaudo, N. R. Kil'deeva and V. G. Babak, *Russ. J. Gen. Chem.*, 2008, **78**, 2239–2246.
- 12 L. Chiappisi, M. Simon and M. Gradzielski, *ACS Appl. Mater. Interfaces*, 2015, **7**, 6139–6145.
- 13 K. Petrak, *J. Bioact. Compat. Polym.*, 1986, **1**, 202–219.
- 14 W. Wang and S. A. Sande, *Langmuir*, 2013, **29**, 6697–6705.
- 15 E. A. Sudbeck, P. L. Dubin, M. E. Curran and J. Skelton, *J. Colloid Interface Sci.*, 1991, **142**, 512–517.
- 16 H. Uchiyama, S. D. Christian, E. E. Tucker and J. F. Scamehorn, *AIChE J.*, 1994, **40**, 1969–1975.
- 17 T. K. Bronich, A. Nehls, A. Eisenberg and A. V. Kabanov, *Colloids Surf., B*, 1999, **16**, 243–251.
- 18 M. Kamimura, J. O. Kim, A. V. Kabanov, T. K. Bronich and Y. Nagasaki, *J. Controlled Release*, 2012, **160**, 486–494.
- 19 H. Katumitu, S. Satoshi, S. Shin-ichiro, S. Iwao and J. C. T. Kwak, *Bull. Chem. Soc. Jpn.*, 1995, **68**, 2179–2185.
- 20 M. Gradzielski, S. Prévost and T. Zemb, *Adv. Colloid Interface Sci.*, 2017, **247**, 374–396.
- 21 M. Gradzielski, A. Rauscher and H. Hoffmann, *J. Phys. IV*, 1993, **3**, C1-65–C1-79.
- 22 M. Odenwald, H.-F. Eicke and W. Meier, *Macromolecules*, 1995, **28**, 5069–5074.
- 23 E. Michel, M. Filiali, R. Aznar, G. Porte and J. Appell, *Langmuir*, 2000, **16**, 8702–8711.
- 24 P. Malo de Molina, C. Herfurth, A. Laschewsky and M. Gradzielski, *Langmuir*, 2012, **28**, 15994–16006.
- 25 M. Schwab and B. Stühn, *J. Chem. Phys.*, 2000, **112**, 6461–6471.
- 26 P. Malo de Molina, M. S. Appavou and M. Gradzielski, *Soft Matter*, 2014, **10**, 5072–5084.
- 27 A. Holmberg, P. Hansson, L. Piculell and P. Linse, *J. Phys. Chem. B*, 1999, **103**, 10807–10815.
- 28 C. Quellet, H. F. Eicke, G. Xu and Y. Hauger, *Macromolecules*, 1990, **23**, 3347–3352.
- 29 J. Koetz, J. Bahnemann, G. Lucas, B. Tiersch and S. Kosmella, *Colloids Surf., A*, 2004, **250**, 423–430.
- 30 J. Baier, J. Koetz, S. Kosmella, B. Tiersch and H. Rehage, *J. Phys. Chem. B*, 2007, **111**, 8612–8618.
- 31 C. Note, J. Koetz and S. Kosmella, *J. Colloid Interface Sci.*, 2006, **302**, 662–668.
- 32 H. Zhang, L. Deng, P. Sun, F. Que and J. Weiss, *J. Colloid Interface Sci.*, 2016, **461**, 88–95.
- 33 E. Buhler, J. Appell and G. Porte, *J. Phys. Chem. B*, 2006, **110**, 6415–6422.
- 34 G. Oetter and H. Hoffmann, *Colloids Surf.*, 1989, **38**, 225–250.
- 35 M. Gradzielski, H. Hoffmann and D. Langevin, *J. Phys. Chem.*, 1995, **99**, 12612–12623.
- 36 M. Gradzielski and H. Hoffmann, *Adv. Colloid Interface Sci.*, 1992, **42**, 149–173.
- 37 M. Gradzielski and H. Hoffmann, *J. Phys. Chem.*, 1994, **98**, 2613–2623.
- 38 B. Farago and M. Gradzielski, *J. Chem. Phys.*, 2001, **114**, 10105–10122.
- 39 M. Gradzielski, *Curr. Opin. Colloid Interface Sci.*, 2004, **9**, 256–263.



- 40 A. Ortega and J. García de la Torre, *J. Chem. Phys.*, 2003, **119**, 9914–9919.
- 41 J. S. Pedersen, D. Posselt and K. Mortensen, *J. Appl. Crystallogr.*, 1990, **23**, 321–333.
- 42 R. J. Baxter, *J. Chem. Phys.*, 1968, **49**, 2770–2774.
- 43 M. J. Grimson, *J. Chem. Soc., Faraday Trans. 2*, 1983, **79**, 817–832.
- 44 L. Baba-Ahmed, M. Benmouna and M. J. Grimson, *Phys. Chem. Liq.*, 1987, **16**, 235–238.
- 45 L. Chiappisi, S. Prévost and M. Gradzielski, *J. Appl. Crystallogr.*, 2014, **47**, 827–834.
- 46 M. Skepo and P. Linse, *Phys. Rev. E*, 2002, **66**, 051807.
- 47 M. Burkhardt, M. Ruppel, S. Tea, M. Drechsler, R. Schweins, D. V. Pergushov, M. Gradzielski, A. B. Zevin and A. H. E. Müller, *Langmuir*, 2008, **24**, 1769–1777.
- 48 K. Pojjak, E. Bertalanits and R. Meszaros, *Langmuir*, 2011, **27**, 9139–9147.
- 49 U. Keiderling and A. Wiedenmann, *Phys. B*, 1995, **213&214**, 895–897.
- 50 K. Lieutenant, P. Lindner and R. Gahler, *J. Appl. Crystallogr.*, 2007, **40**, 1056–1063.
- 51 L. Chiappisi, M. Gradzielski, I. Hoffmann, R. Schweins, M. Simon and H. Yalcinkaya, *Interconnecting charged microemulsion droplets via oppositely charged polyelectrolyte – effect of polyelectrolyte structure*, Institut Laue-Langevin (ILL), 2016, DOI: 10.5291/ILL-DATA.9-12-421.
- 52 U. Keiderling, *Appl. Phys. A*, 2002, **74**, 1455–1457.
- 53 D. Richard, M. Ferrand and G. J. Kearley, *J. Neutron Res.*, 1996, **4**, 33–39.
- 54 I. Breßler, J. Kohlbrecher and A. Thünemann, *J. Appl. Crystallogr.*, 2015, **48**, 1587–1598.

